Available online at www.sciencedirect.com

ScienceDirect

www.elsevier.com/locate/jes

JES JOURNAL OF ENVIRONMENTAL SCIENCES

www.jesc.ac.cn

Long-chain alkanes in the atmosphere: A review☆

Junling Li[1], *Kun Li*[2], *Hong Li*[1,*], *Xuezhong Wang*[1], *Weigang Wang*[3,*], *Ke Wang*[3], *Maofa Ge*[3]

[1] *State Key Laboratory of Environmental Criteria and Risk Assessment, Chinese Research Academy of Environmental Sciences, Beijing 100012, China*

[2] *Laboratory of Atmospheric Chemistry, Paul Scherrer Institute, Villigen 5232, Switzerland*

[3] *State Key Laboratory for Structural Chemistry of Unstable and Stable Species, Beijing National Laboratory for Molecular Sciences, CAS Research/Education Center for Excellence in Molecular Sciences, Institute of Chemistry, Chinese Academy of Sciences, Beijing 100190, China*

ARTICLE INFO

Article history:
Received 12 May 2021
Revised 15 July 2021
Accepted 20 July 2021
Available online 22 February 2022

Keywords:
Long-chain alkanes
Detection methods
Field observation
Laboratory study
Model simulation

ABSTRACT

As a representative species of intermediate volatile organic compounds (IVOCs), long-chain alkanes are considered to be important precursors of secondary organic aerosols (SOA) in the atmosphere. This work reviews the previous studies on long-chain alkanes in the atmosphere: (1) the detection methods and filed observations of long-chain alkanes in both gas and particle phases are summarized briefly; (2) the laboratory studies of long chain alkanes are reviewed, the kinetic data, reaction mechanism, SOA yields, and physicochemical properties of SOA are included in detail; (3) the research progress related to model simulations of long-chain alkanes are also discussed. In addition, based on available research results, several perspective contents are proposed that can be used as a guideline for future research plans.

Introduction

Organic compounds are widely distributed in the atmosphere, such substances enter the atmosphere mainly through the growth, maintenance, and decay of animals, microbes, and plants (Goldstein and Galbally, 2007). The combustion of living or dead organisms can release organic compounds into the atmosphere, such as the consumption of fossil fuel and burning of biomass (Gentner et al., 2017; Hallquist et al., 2009). Due to the difference in molecular weights and functional groups, the volatility and other properties (e.g., optical property, solubility, and reactivity) of the organic compounds are various (Bianchi et al., 2019; Donahue et al., 2012). According to the volatility (in terms of effective saturation concentration, C^*) of the organic compounds, they are grouped into five classes (Donahue et al., 2012): extremely low volatility organic compounds (ELVOCs), with $C^* < 3 \times 10^{-5}$ $\mu g/m^3$; low volatility organic compounds (LVOCs), with $3 \times 10^{-5} < C^* < 0.3$ $\mu g/m^3$; semivolatile organic compounds (SVOCs), with $0.3 < C^* < 300$ $\mu g/m^3$; intermediate volatility organic compounds (IVOCs), with $300 < C^* < 3 \times 10^6$ $\mu g/m^3$; and volatile organic compounds (VOCs), with $C^* > 3 \times 10^6$ $\mu g/m^3$. ELVOCs and LVOCs are mostly in the particle phase (i.e., organic aerosol, OA), VOCs are mostly in the gas phase, and SVOCs and IVOCs can be in either phase mainly determined by their total concentration (Donahue et al., 2012; Pandis et al., 2013). For the organic compound in the gas phase, atmospheric oxidation

☆ This article is dedicated to Professor Dianxun Wang.

* Corresponding authors.
E-mails: lihong@craes.org.cn (H. Li), wangwg@iccas.ac.cn (W. Wang).

https://doi.org/10.1016/j.jes.2021.07.021

can lower their volatility and therefore form secondary organic aerosol (SOA). As OA plays an important role in influencing regional air quality, global climate, and human health (Dominici et al., 2006; Requia et al., 2018), the close relationship between different classes of organic compounds and OA indicates that they play a central role in these environmental processes as well.

Prior to 2007, the formation of SOA is mainly attributed to the oxidation of gas-phase VOCs (Goldstein and Galbally, 2007; Robinson et al., 2007), while EVOCs and IVOCs are generally treated as primary OA (POA) because most of them are in the particle phase when they are freshly emitted. However, the ground-breaking work by Robinson et al. (2007) pointed out that when the fresh emission are diluted in the atmosphere, IVOCs and SVOCs can evaporate to the gas phase and then form a large amount of SOA upon oxidation. Thereafter, IVOCs have attracted much more attention as an important type of SOA precursors (Qi et al., 2019; Zhao et al., 2014). Based on the volatilities of the IVOCs, it is approximately equal to the range of C_{12}-C_{22} *n*-alkanes. Although the components of atmospheric IVOCs are very complex, long-chain alkanes account for a considerable fraction and are frequently considered as the representative substances of IVOCs (Zhao et al., 2014). Long-chain alkanes are mainly emitted by human activities, such as the combustion of fossil fuel, vehicle exhaust, evaporation, etc. (Lamkaddam et al., 2016). Long-chain alkanes are important components of an unresolved complex mixture (UCM) of fossil fuels, a mass of branched alkanes isomers are included as they cannot be separated with traditional gas chromatography-based techniques (Schauer et al., 1999, 2002). For alkanes with multiple carbon atoms, the number of isomers increases exponentially with carbon number (Goldstein and Galbally, 2007), e.g., C_{10} alkane could have 100 possible alkane isomers and most of which could exist in the atmosphere.

As long-chain alkanes have relatively simple structures, they are good target systems for investigating the sensitivity of SOA formation to reaction pathways under various atmospheric oxidation (Lim and Ziemann, 2005). The environmental conditions can affect the SOA yields and chemical compositions derived from long-chain alkanes: temperature can affect the optical properties and chemical compositions of the SOA derived from *n*-dodecane (Li et al., 2020b); the presence of NO_x can change the reaction pathway, and further change the final chemical compositions of the formed SOA (Fahnestock et al., 2015). Chemical structures and molecular sizes of the long-chain alkanes also have important effects on the formation and chemical compositions of SOA (Hunter et al., 2014; Tkacik et al., 2012; Yee et al., 2013): the increasing carbon number of liner alkanes increases of SOA yield (Lim and Ziemann, 2005); the cyclic, liner, and branched alkanes also have different SOA yields (Lim and Ziemann, 2009b). Also, as important representative substances of IVOCs, when long-chain alkanes are considered in the model, the gap between the observed and the modeled SOA formation has been reduced (Zhao et al., 2016).

The atmospheric chemistry of alkanes has been reviewed and evaluated in previous studies (Atkinson, 1990, 1997, 2003; Atkinson and Arey, 2003; Cartier and Atkinson, 1985), and Calvert et al. (2008) summarized the mechanisms of atmospheric oxidation of the alkanes. As far as we know, there is no comprehensive review covering field observation, laboratory experiments, and model simulation related to long-chain alkanes. This review focused on the field, laboratory, and model studies of intermediate volatility long-chain alkanes (C_{12}-C_{22}) in the atmosphere. Section 1 gives a brief review of the detection method of long-chain alkanes. Section 2 reviews field observations that are related to long-chain alkanes. Section 3 summarizes the laboratory studies of long-chain alkanes. Section 4 covers the model studies on long-chain alkanes. Section 5 provides a summary and some recommendations for future research directions on long-chain alkanes.

1. Detection methods

As long-chain alkanes have low atmospheric concentration and low volatility, they are difficult to be analyzed using conventional gas chromatography. The commonly used detection methods of intermediate volatility long-chain alkanes include chemical ionization mass spectrometry (CIMS) and gas chromatography-mass spectrometry (GC-MS) with a preconcentration device.

H_3O^+ CIMS, more commonly known as the proton-transfer-reaction mass-spectrometer (PTR-MS), is one well-established approach to measuring VOCs in the atmosphere (de Gouw and Warneke, 2007; Jordan et al., 2009). VOCs are ionized by transferring the proton from H_3O^+ to the VOCs in the drift tube, $H_3O^+ + R \rightarrow RH^+ + H_2O$. PTR-MS is capable of gaseous organic compounds measurement in atmospheric research. It allows for real-time, online, and determination of absolute concentration measurement of VOCs, the sensitivity of which can reach the low pptv range, and it has a fast response time (in the time range of 40-100 msec) (Graus et al., 2010; Jordan et al., 2009; Sulzer et al., 2014; Yuan et al., 2016). PTR-MS with H_3O^+ can be used to detect alkanes (Erickson et al., 2014; Gueneron et al., 2015). However, only the VOCs whose proton affinity (PA) is larger than that of water (166.5 kcal/mol) can be detected; the PA of alkanes with carbon number $\leq C_8$ is very close to or lower than that of water (Erickson et al., 2014), thus PTR-MS with H_3O^+ can only be used for the measurement of $> C_8$ alkanes and usually lead to a large fraction of fragment ions, the fragment ions distribution and sensitivity of alkanes is a function of the drift conditions (Erickson et al., 2014). Moreover, isomers with the same nominal mass cannot be distinguished, it can only determine the mass-to-charge ratio (*m*/*z*) of the protonated parent ion (or product ion) (Jordan et al., 2009).

CIMS with NO^+ as the reagent ion is the commonly online method used to detect the long-chain alkanes (Amador Muñoz et al., 2016; Erickson et al., 2014; Koss et al., 2016; Ma et al., 2018). The long-chain alkanes react with NO^+ via hydride abstraction, forming ions with *m*/*z* of *m*-1 (where *m* is the molecular mass) (Koss et al., 2016), $NO^+ + R \rightarrow [R-H]^+ + [NO+H]$. Generally, the degree of fragmentation of long-chain alkanes decreases with increasing carbon chain length; for $\geq C_{12}$ alkanes, mass (*m*-1) ions can contribute > 50% of the total ion signals (Koss et al., 2016). Cyclic alkanes, small branched alkanes ($> C_4$, usually C_4-C_8), some important branched alkanes (isopentane and methyl-pentane), and high mass alkanes (C_{12}-C_{15}) can be detected with NO^+ CIMS, forming a

mass (*m*-1) (Koss et al., 2016). In the recent field observation, Ma et al. (2018) measured large alkanes from C_8 to C_{21} with NO^+ proton-transfer-reaction time-of-flight mass spectrometer (PTR-ToF-MS).

GC-MS with a pre-concentration device is also one commonly used equipment to detect the long-chain alkanes in the atmosphere (Chan et al., 2013; Zhao et al., 2013). The pre-concentration device includes Tenax TA adsorbent resin, Teflon bags, SUMA tanks, and filters. The pre-processed samples will be separated by gas chromatography before entering the mass spectrometer for qualitative analysis. To separate and identify complex compounds in the atmosphere, especially for the trace species, such as the isomers of alkanes, two-dimensional gas chromatography (GC × GC) technology is usually applied. This technique provides a direction for the analysis of unidentified complex mixtures and can elute thousands of compounds that can be characterized by mass spectrometry (Chan et al., 2013). The MS connected with the GC can be a time-of-flight mass spectrometer (ToF-MS), which is one soft photoionization MS (Chan et al., 2013; Schnelle-Kreis et al., 2007); can be one PTR-MS (Erickson et al., 2014); can also be the electron impact mass spectrometry (EI-MS), which is a basic mass spectrometer commonly used (Duan et al., 2010; Yao et al., 2009; Zhou et al., 2004). Measurements using the GC interface do not have the fast time response capability compared to CIMS. However, through the separation ability of GC, the fragment ions distribution corresponding to precursor can be mapped, this can be helpful for chemically specific measurement.

2. Field observation

Long-chain alkanes in the atmosphere have biogenic and anthropogenic sources. Biogenic sources include emissions from animal husbandry, plants (e.g., terrestrial higher plants cuticle wax, suspended spores, aquatic plants, and plankton) and microbe, wildfire (e.g., wood and grain straw), etc. (Cao and Jang, 2007; Simoneit, 2002; Yao et al., 2009). Anthropogenic sources include evaporation and burning of fossil fuels (e.g., coal combustion, oil production, evaporation and combustion of fuel oil (gasoline, diesel fuel, kerosene, and motor oil)), volatile chemical products (e.g., pesticides, detergents, paints, printing inks, personal care products), etc. (Huang et al., 2018; Jathar et al., 2017; Lou et al., 2019; Robinson et al., 2007; Schauer et al., 2002; Wu et al., 2019).

In urban areas, long-chain alkanes are mainly from vehicle emissions, including diesel exhaust and gasoline exhaust (Liu et al., 2017; Luo et al., 2019; Zhao et al., 2015), especially in winter. Moreover, cargo vessels (Huang et al., 2018) and aircraft (Agrawal et al., 2008) are also important contributors to long-chain alkanes emissions in the atmospheric environment.

Schauer et al. (1999) reported the alkane emissions from medium-duty diesel trucks and found that the gas-phase alkanes were emitted at a rate of 11.2 mg/km driven, and were in the carbon number range from C_{12} to C_{20}. During this carbon number range, n-alkane emission rates were greatest, averaging over 400 μg/km for most of the individual n-alkanes. For individual organic compounds in the class of branched alkanes (C_{14} to C_{20}), they were emitted at rates of 360-750 μg/km. For light-duty diesel vehicles, Siegl et al. (1999) found that C_{12}-C_{20+} hydrocarbons accounted for 20% of the total emitted non-methane hydrocarbons in the gas phase, implying the important role of long-chain alkanes in vehicle emissions.

de Gouw et al. (2011) reported the importance of IVOCs for SOA formation based on airborne measurements of the Deepwater Horizon Oil Spill. They found that species with the evaporation of about $C^* = 10^5$ mg/m^3 (C_{14} to C_{16} hydrocarbons) were the most likely precursors of observed SOA. Liggio et al. (2016) provided one quantitative assessment of the magnitude of SOA formation from oil sand emissions. Airborne measurements, laboratory experiments, and a box model simulation were used over the Canadian oil sands. They found that the evaporation and oxidation of low volatility organic vapors (I/SVOCs; with alkanes as the majority components) from the mined oil sands were important sources of observed SOA in the atmosphere. The results suggest that the oil sand emitted I/SVOCs should be considered in the field observations and model simulations.

Long-chain alkanes have been proposed as important SOA contributors in urban areas (Robinson et al., 2007; Yuan et al., 2013; Zhao et al., 2014), which can produce SOA as much as (or more than) polycyclic aromatics and single ring aromatics from vehicle emissions (Deng et al., 2017; Liggio et al., 2016; Liu et al., 2017; Luo et al., 2019; Yuan et al., 2013; Zhao et al., 2015). Yuan et al. (2013) measured the VOCs on Changdao Island in China and found that polycyclic aromatic hydrocarbons (PAHs) and higher alkanes (> C_{10}) could contribute to 17.4% of the SOA formation during the campaign. They emphasized the importance of I/SVOCs measurements in the atmosphere. Wu and Xie (2018) estimated the secondary organic formation potential (SOAFP) of AVOCs based on the updated speciated VOC emission inventory in China in 2013. They found that although the emissions of *n*-dodecane, *n*-decane, and *n*-undecane contribute small fractions in concentrations (1.3%, 1.0%, and 0.7%), they accounted for 11.4, 4.6%, and 4.6% of the nationwide's total SOAFP due to their higher SOA yields. Wang et al. (2020b) estimated the long-chain alkanes (C_{12}-C_{22}) emissions from vehicles for the Yangtze River Delta region (YRD) during 2017 and found that C_{12}-C_{22} alkanes emissions from diesel-powered vehicles were much higher than those from gasoline-powered vehicles: the mass fraction of C_{12}-C_{22} alkanes in total IVOCs were 57.27 μg/mg for diesel-powered vehicles and 27.99 μg/mg for gasoline-powered vehicles. They also emphasized the contribution of long-chain alkanes to SOA generation. These studies further recognized the contribution of long-chain alkanes to SOA generation in the atmosphere.

The measurements related to long-chain alkanes have become more and more recognized. Researchers have learned much about long-chain alkanes in the atmosphere, in both the particle phase and gas phase. **Table 1** summarizes the observed concentrations of long-chain alkanes in the atmosphere (in both phases).

2.1. *Atmospheric particle-phase observation*

For the analysis of long-chain alkanes in the particle phase, the methods are mainly membrane collection and offline

Table 1 – The concentration of long-chain alkanes (≥C_{12}) in different sites worldwide in various studies.

Locations Compounds	PRD [a], China Alkanes[d]	NCP [b], China Alkanes[d]	Paris, France *n*-Alkanes[e]		Pasadena, USA Alkanes[f]	London[c], UK *n*-Alkanes[g]	
Methods	NO^+ PTR-ToF-MS	NO^+ PTR-ToF-MS	TD-GC-FID		TD-GC-MS	TD-GC × GC-ToF-MS	
Sample Time	Sept.-Nov. 2018	Nov.-Dec. 2018	Jul. 2009	Jan.-Feb. 2010	May -Jun. 2010	Mar. - Apr. 2017	
Phases	Gas (pptV)	Gas (pptV)	Gas (pptV)	Gas (pptV)	Gas (pptV)	Gas (pptV)	Particle (pptV)
Dodecane	122±120	129±86	22±21	7±4	8±1	–	–
Tridecane	66±60	89±59	13±12	2±1	6±1	4.13	0.17
Tetradecane	50±47	57±39	27±23	2±2	9±2	3.43	0.25
Pentadecane	45±42	46±33	23±18	4±2	5±0.8	4.01	0.16
Hexadecane	36±33	32±24	22±19	ND[h]	4±1	3.20	0.37
Heptadecane	21±20	18±14	–	–	3±0.4	1.93	0.02
Octadecane	13±14	11±9	–	–	1.6±0.5	2.61	0.12
Nonadecane	5±9	4±7	–	–	0.7±0.2	0.46	0.33
Eicosane	0.7±4	3±6	–	–	0.24±0.08	0.19	0.33
Heneicosane	0.5±5	2±5	–	–	0.15±0.1	0.19	0.90
Docosane	–	–	–	–	–	0.27	0.98
Tricosane	–	–	–	–	–	0.52	0.99
Tetracosane	–	–	–	–	–	0.49	0.88
Pentacosane	–	–	–	–	–	0.31	0.57
Hexacosane	–	–	–	–	–	0.16	0.33
Heptacosane	–	–	–	–	–	0.08	0.46
Octacosane	–	–	–	–	–	0.02	0.38
Nonacosane	–	–	–	–	–	0.01	0.52
Triacontane	–	–	–	–	–	0.01	0.35
Hentriacontane	–	–	–	–	–	0.004	0.39
Dotriacontane	–	–	–	–	–	–	0.43
Tritriacontane	–	–	–	–	–	–	0.37
Tetratriacontane	–	–	–	–	–	–	0.03

[a] the Pearl River Delta (PRD) region in China, urban area;
[b] the North China Plain (NCP) region in China, suburban area;
[c] Samples are collected at the kerbside MR Supersite on the south side of Marylebone Road, urban area;
[d] Wang et al. (2020a); [e:] Ait-Helal et al. (2014); [f:] Zhao et al. (2014); [g:] Xu et al. (2020);
[h] Not detected.

analysis. Usually, the particles are collected with a particle sampler, and then the extracted samples are analyzed with GC-MS. N-alkane (> C_{12}) is one of the key components of particle-phase analysis. Carbon preference indices (CPI) derived from GC analyses are widely used as a cue of n-paraffins distributions to recognition of source beds (Bray and Evans, 1961). According to CPI values, the sources of n-alkanes are identified: the larger the CPI value, the greater the contribution of biological sources (CPI > 5); conversely, the greater the impact of anthropogenic sources (fossil fuel, CPI ~1); the CPI value of mixed source alkanes varies with the relative contribution of biogenic sources and anthropogenic sources (Simoneit and Mazurek, 1982).

Based on CPI values, previous field observation studies showed that n-alkanes in the particle phase in Beijing are mainly from anthropogenic sources (e.g., coal and fossil fuel combustion) in winter (Kang et al., 2018; Li et al., 2013; Ma et al., 2013; Yao et al., 2009; Zhou et al., 2004), while in spring and summer, the n-alkanes from biogenic origins (e.g., plant wax) should also be considered (Duan et al., 2010; Kang et al., 2018; Li et al., 2015). Schnelle-Kreis et al. (2007) found that n-alkanes (C_{20}-C_{34}) of German urban areas in winter showed a good positive correlation with anthropogenic sources (e.g., lubricating oi, emissions of unburned diesel and heating oil consumption, wood combustion, brown coal combustion), while in summer, it showed a positive correlation with biogenic emissions and transport components. Charron et al. (2019) identified and quantified key species of exhaust and non-exhaust vehicle emissions, results found that C_{19}-C_{26} n-alkanes were important in roadside concentration increments. The CPI was close to unity 0.99, this indicated the equal distribution of typical anthropogenic emissions between odd and even carbon numbers. Observations above showed that with the alternation of seasons, biogenic emission and people's lifestyles (e.g., heating, transportation) will change, resulting in changes of the corresponding emission sources; this indicates that the sources of particle-phase n-alkanes are influenced by the alternation of seasons.

Emission factors (EF) is one calculation method for the particle pollutants in the roadway tunnel, this method is described in detail by Pierson et al. (1996):

$$EF = (C_{out}V_{out} - C_{in}V_{in})/NL$$

where EF is the emission factor of a species for tests in the unit of mg/(vehicle•km); C_{out} is the measured species concentration at the tunnel outlet, and C_{in} is the measured species concentration at the tunnel inlet; V is the calculated air volume; N is the vehicle numbers passing through the tunnel; L is the distance between two sampling locations. Emission

factors of NO_x are also one estimated method for the analysis of n-alkanes in the related road emission observations. The concentration of roadside NO_x can be treated as one dispersion tracer, as the roadside increments of $PM_{2.5}$, $PM_{2.5\text{-}10}$, and PM_{10} correlate strongly with roadside NO_x (Jones and Harrison, 2006), details of calculation processes can be referred to Jones and Harrison (2006).

He et al. (2008) analyzed the $PM_{2.5}$ emissions from on-road vehicles in the Zhujiang Tunnel in the PRD region of China in September in 2004 with GC-MS, the EF calculation method is applied. Hydrocarbons with C_{16}-C_{32} (*n*-alkanes) in the $PM_{2.5}$ emissions were determined with the EF value and the total emission factor of which was determined to be 359 μg/(vehicle•km). Perrone et al. (2014) reported that the n-alkanes (C_{20}–C_{32}) were the most abundant trace organic compounds in particulate species of vehicle exhaust (Euro 1-4 light-duty vehicles were included), the EF values were in the range of 101-2034 μg/(vehicle•km). Charron et al. (2019) reported the *n*-alkanes EF values in the particle phase of both the roadside observations and the lab tests; the measurement was at the roadside of Grenoble Ring Road in Grenoble, France, the median EF values of n-alkanes (C_{19}–C_{26}) were in the range of 31.4-133.99 μg/(vehicle•km) for Euro 3 and 4 types of diesel; for lab-tested diesel passenger car median concentration, EF value of *n*-alkanes (C_{19}–C_{26}) was 134 μg/(vehicle•km) for Euro 3, 31.3 μg/(vehicle•km) for Euro 4. Xu et al. (2020) analyzed the hydrocarbons in the particle phase in central London from March 22 to April 18 in 2017, results showed that the EF value of n-alkanes (C_{13}-C_{34}) was 675.48 μg/(vehicle•km). Due to the differences in traffic fleet compositions around the world, the EF values observed in different regions may be different.

For long-chain alkanes in the particle phase, the analyzing methods may be different due to the different sampling locations, sampling methods, and detection methods. Nevertheless, all previous studies have concluded that anthropogenic sources have a significant impact on long-chain alkanes in particles, especially in urban areas.

2.2. *Atmospheric gas-phase observation*

With the development of detection technology, the detection method for gas-phase long-chain alkanes has gradually transferred from offline sampling and analysis (e.g., thermal desorption-gas chromatography coupled to a flame ionization detector, TD-GC-MS) to online detection (e.g., NO^+ chemical ionization in proton transfer reaction time-of-flight mass spectrometry, NO^+ PTR-ToF-MS).

TD-GC-MS is one commonly used equipment for online detection of long-chain alkanes in the atmosphere. Ait-Helal et al. (2014) measured the n-alkanes (C_{12}-C_{16}) in the gas phase with TD-GC-FID in suburban Paris in 2009 and 2010. Results showed that the n-alkanes concentrations in summer were higher than that in winter, suggesting that the gas-particle partitioning theory is not applicable here. They also found that the n-alkanes (C_{12}-C_{16}) could explain 2%-7% of the SOA formation, which was half of the contribution of traditional aromatic compounds (15%), emphasizing the importance of the n-alkanes in SOA formation. Zhao et al. (2014) analyzed the alkanes with TD-GC-MS during the CalNex study from May 15 to June 11, 2010, in Pasadena, USA. They found that in addition to road diesel vehicles, other petroleum-related emission sources greatly increased IVOCs (e.g., long-chain alkanes) emissions. Xu et al. (2020) measured long-chain alkanes in the gas phase in central London from March 22 to April 18 in 2017 with TD-GC × GC-ToF-MS. They found that lower molecular weight hydrocarbons from C_{13} to C_{18} were primarily in the gas phase, and the peak abundance of hydrocarbons from C_{10} to C_{20} was mainly attributed to diesel fuel.

Now, NO^+ PTR-ToF-MS is a relatively new equipment for detecting long-chain alkanes. Wang et al. (2020a) performed the high-time-resolution (10 sec) measurements of long-chain alkanes with NO^+ PTR-ToF-MS at a rural site in Baoding in the NCP and at an urban site in Guangzhou in the PRD from September to November in 2018. High concentrations of long-chain alkanes were observed in both urban and rural environments in China, and their SOA production was comparable to or higher than naphthalenes and single-ring aromatics. The diurnal profiles of long-chain alkanes in the gas phase were similar to anthropogenic VOCs (e.g., benzene), indicating that they were mainly from anthropogenic sources. They emphasized the necessity to include long-chain alkanes in the model for SOA formation.

According to the results above, diesel-powered vehicles have an important impact on urban air quality; vehicle type, fuel composition, road conditions, vehicle speed, etc. can affect the long-chain alkanes emission and concentration in the gas phase. As long-chain alkanes have a significant contribution to SOA formation, more attention should be paid to their concentrations (in addition to traditional VOCs) during field observations.

3. Laboratory study

Long-chain alkanes in the troposphere are mainly transformed by the chemical reactions with hydroxyl (OH) radical and Cl atoms; the reaction with NO_3 radical is so slow that it can be ignored, and no reaction with O_3 has been observed (Atkinson and Arey, 2003). In this part, laboratory studies of long-chain alkanes with $\geq$12 carbons are summarized; kinetic data, reaction mechanism, and SOA yield and physicochemical properties are included.

3.1. *Kinetic data*

Reactions of long-chain alkanes with OH radical typically occur during daylight hours (Young et al., 2014). Kinetics of the gas reactions of the OH radicals with alkanes in the troposphere are discussed in previous reviews in detail (Atkinson, 1997, 2000, 2003; Atkinson and Arey, 2003). Here we summarize these kinetic data from these reviews together with some updates from more recent studies (Lamkaddam et al., 2019; Shi et al., 2019a).

Temperature-dependent rate expressions are given as the Arrhenius expression:

$$k(T) = A(T/298\ \mathrm{K})^n e^{-E_a/RT} \quad (1)$$

The rate constants of long-chain alkanes with OH radical are listed in **Table 2**, which consists of C_{12}-C_{16} alkanes. The available temperature-dependent parameters and applicable

Table 2 – Rate constants (k) of long-chain alkanes with OH radicals.

Organic	k (298 K) ($\times 10^{-11}$ cm^3/(molecule•sec))	Methods	References
n-Dodecane	1.39	Evaluation methods	Atkinson, 2003
	1.29±0.02 (300 K)	Relative rate methods (RR) (relative to k(*n*-octane) = 8.15 × 10^{-12})	Behnke et al., 1988
	1.40±0.05 (312 K)	RR (relative to k(*n*-heptane) = 6.97 × 10^{-12})	Nolting et al., 1988
	1.27±0.31 (283 K)	RR (relative to k(Isoprene) = (1.07±0.31) × 10^{-10})	Lamkaddam et al., 2019
	1.33±0.34 (293 K)	RR (relative to k(Isoprene) = (1.02±0.15) × 10^{-10})	Lamkaddam et al., 2019
	1.27±0.40 (303 K)	RR (relative to k(Isoprene) = (0.98±0.15) × 10^{-10})	Lamkaddam et al., 2019
2-Methyl undecane	1.31±0.07 (297 K)	RR (relative to k(*n*-dodecane) = 1.39 × 10^{-11})	Loza et al., 2014
3,6-Dimethyl decane	1.45	SAPRC-99 mechanism	Carter, 2000; Carter et al., 2002
5-Methyl undecane	1.43	SAPRC-99 mechanism	Carter, 2000; Carter et al., 2002
3-Methyl undecane	1.43	SAPRC-99 mechanism	Carter, 2000; Carter et al., 2002
n-Hexyl cyclohexane	1.74±0.06 (297 K)	RR (relative to k(*n*-dodecane) = 1.39 × 10^{-11})	Loza et al., 2014
	1.78 (300K)	SAPRC-99 mechanism	Carter, 2000; Carter et al., 2002
	1.31	Evaluation methods	Fahnestock et al., 2015
1,3,5-Triethyl cyclohexane	1.90	SAPRC-99 mechanism	Carter, 2000; Carter et al., 2002
1-Methyl-4-pentyl cyclohexane	1.80	SAPRC-99 mechanism	Carter, 2000; Carter et al., 2002
Cyclododecane	1.47±0.04 (297 K)	RR (relative to k(*n*-dodecane) = 1.39 × 10^{-11})	Loza et al., 2014
	1.47	Evaluation methods	Fahnestock et al., 2015
n-Tridecane	1.51	Evaluation methods	Atkinson, 2003
	1.62±0.06 (312 K)	RR (relative to k(*n*-heptane) = 6.97 × 10^{-12})	Nolting et al., 1988
	1.60	SAPRC-99 mechanism	Carter, 2000; Carter et al., 2002
	1.44±0.02 (300 K)	RR (relative to k(*n*-octane) = 8.15 × 10^{-12})	Behnke et al., 1988
3,6-Dimethyl undecane	1.60	SAPRC-99 mechanism	Carter, 2000; Carter et al., 2002
5-Methyl dodecane	1.57	SAPRC-99 mechanism	Carter, 2000; Carter et al., 2002
3-Methyl dodecane	1.57	SAPRC-99 mechanism	Carter, 2000; Carter et al., 2002
n-Heptyl cyclohexane	1.91	SAPRC-99 mechanism	Carter, 2000; Carter et al., 2002
1,3-Diethyl-5-pentyl cyclohexane	2.05	SAPRC-99 mechanism	Carter, 2000; Carter et al., 2002
1-Methyl-2-hexyl-cyclohexane	1.94	SAPRC-99 mechanism	Carter, 2000; Carter et al., 2002
n-Tetradecane	1.67	Evaluation methods	Sivaramakrishnan and Michael, 2009
	1.79±0.07 (312 K)	RR (relative to k(*n*-heptane) = 6.97 × 10^{-12})	Nolting et al., 1988
	1.80	SAPRC-99 mechanism	Carter, 2000; Carter et al., 2002
3,7-Dimethyl dodecane	1.74	SAPRC-99 mechanism	Carter, 2000; Carter et al., 2002
6-Methyl tridecane	1.71	SAPRC-99 mechanism	Carter, 2000; Carter et al., 2002
3-Methyl tridecane	1.71	SAPRC-99 mechanism	Carter, 2000; Carter et al., 2002
n-Octyl cyclohexane	2.05	SAPRC-99 mechanism	Carter, 2000; Carter et al., 2002
1,3-Dipropyl-5-ethyl cyclohexane	2.19	SAPRC-99 mechanism	Carter, 2000; Carter et al., 2002
1-Methyl-4-heptyl cyclohexane	2.08	SAPRC-99 mechanism	Carter, 2000; Carter et al., 2002
n-Pentadecane	1.81	Evaluation methods	Sivaramakrishnan and Michael, 2009
	1.72±0.18	RR (relative to k(toluene) = (6.40±0.64) × 10^{-12} and k(*m*-xylene) = (240 ± 0.25) × 10^{-11})	Shi et al., 2019a
	2.07±0.10 (312 K)	RR (relative to k(*n*-heptane) = 6.97 × 10^{-12})	Nolting et al., 1988
	2.10	SAPRC-99 mechanism	Carter, 2000; Carter et al., 2002
3,7-Dimethyl tridecane	1.88	SAPRC-99 mechanism	Carter, 2000; Carter et al., 2002
6-Methyl tetradecane	1.85	SAPRC-99 mechanism	Carter, 2000; Carter et al., 2002
3-Methyl tetradecane	1.85	SAPRC-99 mechanism	Carter, 2000; Carter et al., 2002
2,6,10-Trimethyl dodecane	1.90±0.20	RR (relative to k(toluene) = (6.40±0.64) × 10^{-12} and k(*m*-xylene) = (240 ± 0.25) × 10^{-11})	Shi et al., 2019a
n-Nonyl cyclohexane	2.09±0.22	RR (relative to k(toluene) = (6.40±0.64) × 10^{-12} and k(*m*-xylene) = (240 ± 0.25) × 10^{-11})	Shi et al., 2019a
	2.20	SAPRC-99 mechanism	Carter, 2000; Carter et al., 2002
1,3,5-Tripropyl cyclohexane	2.33	SAPRC-99 mechanism	Carter, 2000; Carter et al., 2002
1-Methyl-2-octyl cyclohexane	2.22	SAPRC-99 mechanism	Carter, 2000; Carter et al., 2002
n-Hexadecane	1.94	Evaluation methods	Sivaramakrishnan and Michael, 2009
	2.32±0.13 (312 K)	RR (relative to k(*n*-heptane) = 6.97 × 10^{-12})	Nolting et al., 1988

Table 3 – Temperature-dependent parameters and applicable temperature range for long-chain alkanes with OH radical.

Organic	Temperature (K)	A (10^{-11} cm^3/(molecule•sec))	*n*	E_a (kJ/mol)	References
n-Dodecane	298-2000	2.21	0.96	1.16	Carter et al., 2002; Sivaramakrishnan and Michael, 2009
n-Tridecane	298-2000	2.65	0.91	1.36	Sivaramakrishnan and Michael, 2009
n-Tetradecane	298-2000	3.09	0.86	1.52	Sivaramakrishnan and Michael, 2009
n-Pentadecane	298-2000	3.55	0.82	1.67	Sivaramakrishnan and Michael, 2009
n-Hexadecane	298-2000	4.01	0.79	1.80	Sivaramakrishnan and Michael, 2009

Table 4 – Rate constants of long-chain alkanes with Cl atom.

Organic	*k* (298 K) (10^{-10} cm^3/(molecule•sec))	Methods	References
n-Dodecane	5.12±0.29	RR (relative to trans-2-butene, m-xylene and ethylbenzene)	Shi et al., 2019b
	5.36	RR (relative to n-butane)	Aschmann and Atkinson, 1995
n-Tridecane	5.30±0.30	RR (relative to trans-2-butene, m-xylene and ethylbenzene)	Shi et al., 2019b
n-Tetradecane	5.68±0.34	RR (relative to trans-2-butene, m-xylene and ethylbenzene)	Shi et al., 2019b

temperature range for the long-chain alkanes with OH radical are listed in **Table 3**.

Compared with the alkenes and aromatic hydrocarbons' fast reactions with OH radicals (Atkinson and Arey, 2003), the reactivities of long-chain alkanes with OH radicals are slow to medium. This results in one phenomenon that little of the long-chain alkanes is oxidized in urban areas close to their emission points, the remainder can be transported over a large distance within the atmospheric boundary layer into the environment downwind of the source regions. The transported environments can be chemically different from the urban areas. Therefore, it is necessary to consider more reaction initiators for alkanes, e.g., Cl in the marine boundary layer.

The reactions of long-chain alkanes with Cl atoms mainly occur during daylight hours in coastal and marine areas. Cl atoms have relatively high reactivity, the existing research mainly focuses on the reactions with volatile organic compounds (VOCs), the reaction rate constants of VOCs with Cl atoms are usually 1–2 order of magnitude larger than those with OH radicals (Bejan et al., 2018; Shi et al., 2019b). In contrast, the reactions of Cl atoms with IVOCs (e.g., long-chain alkanes) are relatively few. The available rate constants of long-chain alkanes with Cl atoms are listed in **Table 4**.

Although, the reaction rates of alkanes with NO_3 radical are slow, the concentrations of NO_3 radical in the atmosphere are much higher than those of OH radicals and Cl atoms, especially at nighttime. The importance of these reactions could not be ignored. As this work mainly summarized the studies related to C_{12}-C_{22} alkanes, and the existing studies mainly focus on alkanes below C_{10}, thus we added the content of the reactions of alkanes below C_{10} with NO_3 to supplementary.

3.2. *Reaction mechanism*

The general mechanism for long-chain alkanes with OH radical is shown in **Fig. 1**, under low-NO_x conditions (Yee et al., 2012, 2013) (**Fig. 1a**) and high-NO_x conditions (Aimanant and Ziemann, 2013; Lim and Ziemann, 2005, 2009a, 2009b) (**Fig. 1b**). According to existing literature, the reaction of long-chain alkanes (RH) begins with H-abstraction by OH radical from parent alkanes to form an alkyl peroxy radical (RO_2). Usually, H-abstraction occurs predominantly at secondary H atoms, as the stability at the radical site from electron-donating alkyl groups is enhanced. As revealed by **Fig. 1a**, under low NO_x conditions, the fate of RO_2 is dominated by reaction with HO_2 to form hydroperoxide (ROOH). The ROOH has three reaction channels: channels 1 and 2 are the reactions with OH radical, while channel 3 is photolysis. For channel 1, the ROOH reacts with OH radical and forms the carbonyl compound (CARB), which can be further oxidized to the carbonyl hydroperoxide compound (CARBROOH). For channel 2, the ROOH reacts with OH radical to form dihydroperoxide (DIROOH) and carbonyl hydroperoxide (CARBROOH). The CARBROOH can then undergo channel 2a or 2b to form higher functionalized products, or it can react with the fragmentation products (e.g., ALD from channel 1) to from carbonyl hydroperoxide peroxyhemiacetal (CARBROOHPHA), this is also the reaction of channel 1b. The CARBROOH and higher functionalized products and CARBROOHPHA can partition into the particle phase. The photolysis reactions can also occur for CARBROOH, resulting in the formation of fragmentation products: aldehyde (ALD), peracid (CnPACID), hydroperoxides (CnROOH), and carboxylic acid (CnCARBACID) (channel 1a). In channel 3, the ROOH undergoes photolysis to form alkoxy radical (RO), and then RO undergoes a 1,4-isomerization reaction to form 1,4-hydroxy hydroperoxide (OHROOH). OHROOH can partition into the particle phase, as it has sufficiently low volatility. OHROOH can also react with OH radical or undergo photolysis to form OHCARB (Yee et al., 2013). The OHCARB can undergo cyclization under acid catalysis to form a cyclic hemiacetal (CHA) and a dihydrofuran (DHF) with dehydration process in the particle phase. For long-chain alkanes with different chemical structures, the location of H-abstraction will be different, and this will result in different products (Yee et al., 2012). Generally, long-chain alkanes with branched structures lead to fragmentation and form more volatile products, while long-chain alka-

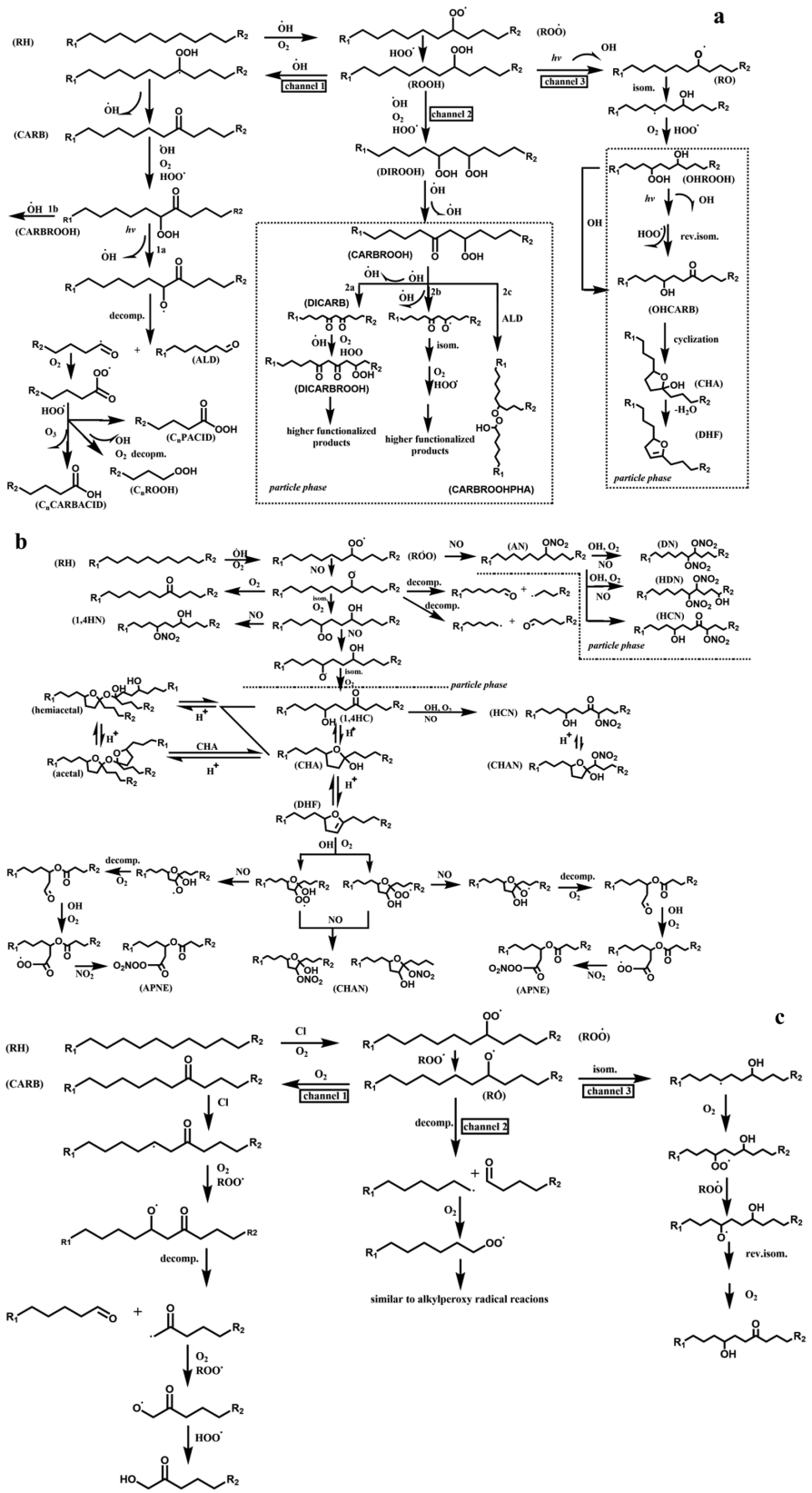

Fig 1 – The general mechanism for long-chain alkanes: (a) OH oxidation under low-NO_x conditions; (b) OH oxidation under high-NO_x conditions; (c) reaction with Cl atom.

nes with cyclic structures will undergo faster oxidation and form less volatile products (Yee et al., 2013).

For the reaction mechanism of long-chain alkanes under high-NO_x conditions, the fate of RO_2 is dominated by reaction with NO to form an alkoxy radical (RO) or an alkyl nitrate (AN) (Aimanant and Ziemann, 2013; Lim and Ziemann, 2005, 2009a). The AN can react with NO and OH to form dinitrate (DN), hydroxydinitrate (HDN), and hydroxycarbonyl nitrates (HCN). The RO radical can be decomposed to form aldehydes and alkyl radicals, and then proceed to the gas phase reactions. This reaction process is important, as the products formed tend to exist in the gas phase and lead to the reduction in particle formation. In addition to the decomposition, the RO can react with O_2 to form a carbonyl compound and can isomerize through a 1,5-H atom shift process to form a 1,4-hydroxyperoxy radical. The 1,4-hydroxyperoxy radical reacts with NO to form a 1,4-hydroxynitrates (1,4HN) or a 1,4-hydroxyalkoxy radical. The 1,4-hydroxyalkoxy radical mainly isomerizes to form a 1,4-hydroxycarbonyl compound (1,4HC). The 1,4HC compounds can partition into particle phase and on the chamber walls, where they can isomerize to form cyclic hemiacetals (CHA). The CHA can generate dihydrofuran (DHF) by dehydration, and the formed DHF can evaporate to the gas phase again (Martin et al., 2002). The DHF can react with OH radical rapidly via addition to the C=C double bond, and then the formed intermediate products can react with NO to form cyclic hemiacetal nitrates (CHAN) or to form acylperoxynitrate esters (APNE) through decomposition and the reaction with NO_2. 1,4HC compounds can also react with NO to form hydroxycarbonyl nitrates (HCN) and cyclic hemiacetal nitrates (CHAN). With the catalysis of protons, 1,4HC can react with CHA to form hemiacetal and acetal. For alkanes with different structures, the reaction mechanisms are similar; however different structures of which can lead to different branching ratios for the reaction pathways (Lim and Ziemann, 2009a). Compared with cyclic and n-alkanes, branched alkanes are more prone to decomposition reactions and produce products with higher volatility (Lim and Ziemann, 2009a).

The reaction mechanism of Cl atoms with long-chain alkanes is similar to that of OH oxidation under low-NO_x conditions. According to available literature, the reactions for *n*-undecane, *n*-dodecane, tridecane, and tetradecane with Cl atoms are a little different, as their reactions do not produce products that retain the carbon chain (Shi et al., 2019b), producing small molecule products with the decomposition process. As shown in **Fig. 1c**, the reaction is initiated by removing H atoms with Cl atoms to generate alkyl radicals, and the alkyl radicals then react with oxygen to form RO_2. The fate of RO_2 is dominated by reaction with RO_2 to form RO. RO radicals mainly have three reaction channels. For channel 1, the RO radical reacts with O_2 to form carbonyl compound and HO_2, and then the carbonyl compound will continue to react with Cl atoms. Channel 2 is the decomposition of RO radicals, generating small molecules. For channel 3, the RO radicals undergo an intramolecular hydrogen transfer reaction, generating hydroxy carbonyl compounds.

In addition to the reactants, environmental factors can also affect the reaction mechanism of long-chain alkanes, e.g., relative humidity (RH), aerosol acidity, and temperature. Li et al. (2020b) performed the low-NO_x photo-oxidation with C12 alkanes under room (25°C) and low temperature (5°C) conditions and found that low-temperature conditions could promote the formation of oligomers in the particle phase. It was also found that the humidity can affect the partitioning of the formed products (Tobias et al., 2000), and the aerosol acidity can affect the reaction process of aldehydes and ketones (Jang et al., 2002).

3.3. *SOA formation*

3.3.1. *SOA yield*

SOA yield is an important parameter for model simulation and laboratory research. **Fig. 2** lists the SOA yields derived from long-chain alkanes under various conditions. The oxidant type, NO_x concentrations, the carbon numbers and structure of alkanes, reaction time, environmental conditions (e.g., temperature, relative humidity, etc.), and aerosol acidity can all affect the SOA yields.

The SOA yields can be affected by the precursor types and structures. Lim and Ziemann (2005, 2009b) reported that SOA yields for long-chain alkanes from reactions of homologous series increased monotonically with increasing carbon atom number, due to the decreasing volatility of the long-chain alkanes and thus the formed products. For a given carbon atom number, SOA yields follow the order cyclic > linear > branched, which is determined by the decomposability extent of the alkoxy radical intermediates and the volatility of the products. Tkacik et al. (2012) found that branched alkanes had the lowest SOA yields among alkanes with the same carbon number but different structures and the SOA yields of branched alkanes depended on the methyl branch position on the carbon backbone. Fahnestock et al. (2015) also reported that structure played a key role in determining the degree of fragmentation and functionalization of the alkanes.

The type of oxidant and the oxidation time can also affect the SOA yields. Lambe et al. (2012) found that the SOA yields of long-chain alkanes exhibited an increasing trend followed by a decreasing trend as a function of OH exposure, likely due to that the transit of products from functionalization (oxygen addition) to fragmentation (carbon loss). Loza et al. (2014) reported the SOA yields for C_{12} alkanes and found that gas-phase fragmentation was more prevalent under high-NO_x conditions than under low-NO_x conditions. Fahnestock et al. (2015) found that under high-NO conditions, the formed organonitrate could increase the aerosol volume concentration by up to a factor of 5 compared with the low-NO condition.

Environmental conditions can also affect SOA yields. Lamkaddam et al. (2020) reported that from dry (<1%) to humid (≥5%) conditions, SOA yields were reduced by a factor of 2 for the high-NO_x OH oxidation of *n*-dodecane; under dry conditions, the acid-catalyzed "dehydration" reactions of polyfunctional molecules could lead to the formation of lower volatility products, while the higher humidity could inhibit this reaction pathway. Lamkaddam et al. (2016) also investigated the temperature effect on SOA yields derived from *n*-dodecane in the presence of NO_x at 10-31.5°C. They found that the temperature does not significantly affect the SOA formation in these experiments, indicating that the formed SOA is dominated by extremely low volatility prod-

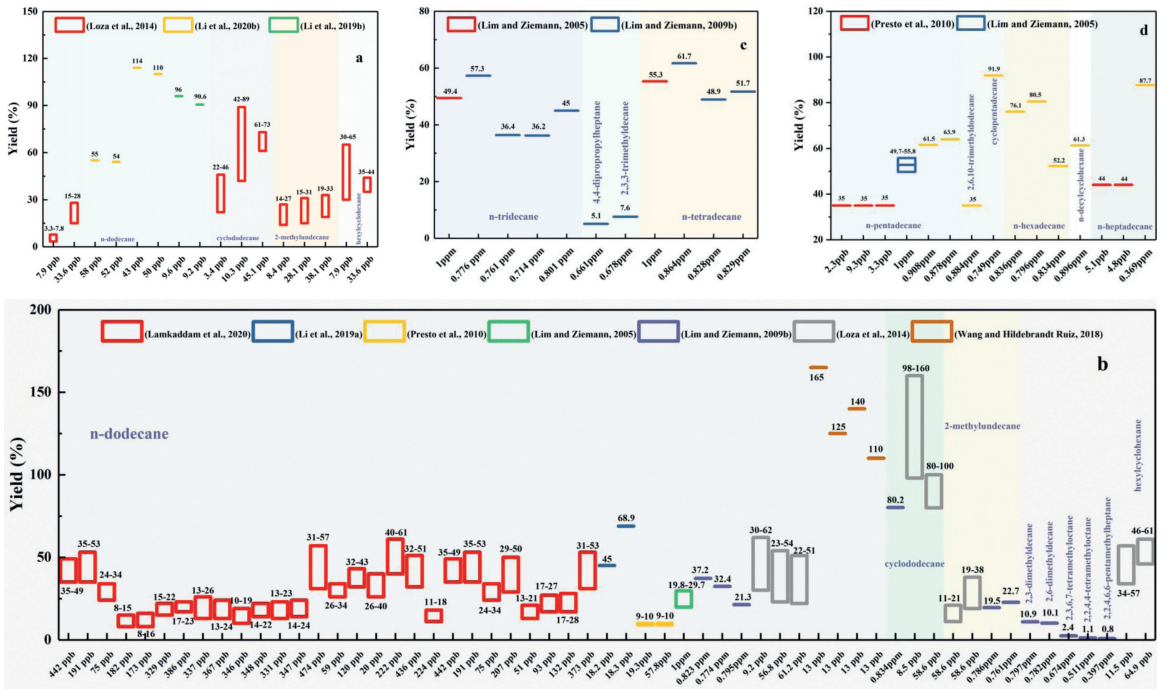

Fig 2 – SOA yields derived from long-chain alkanes under various conditions: (a) C_{12} alkanes under low-NO_x conditions; (b) C_{12} alkanes under high-NO_x conditions; (c) C_{13} and C_{14} alkanes under high-NO_x conditions; (d) C_{15}, C_{16}, and C_{17} alkanes under high-NO_x conditions. Details of the reaction conditions can be referred to Table S2 **(Li et al., 2019a, 2019b; Presto et al., 2010; Wang and Hildebrandt Ruiz, 2018).**

ucts. Li et al. (2020b) reported that the temperature had an important effect on the SOA formation derived from *n*-dodecane under low-NO_x conditions: higher SOA formation was found under low-temperature conditions. The mass spectrometry analysis revealed that low-temperature conditions could promote the formation of oligomers, which led to higher SOA yields under low-temperature conditions. The different temperature effects under low- and high-NO_x conditions highlight the important role of NO_x in the formation of alkane SOA.

3.3.2. *Physicochemical properties of SOA*

The physicochemical properties of SOA derived from long-chain alkanes mainly summarize optical property and density here. The optical property of SOAs mainly depends on the complex refractive index (RI, $n + ki$), which can express the extent of light-absorbing (the imaginary part, *k*) and scatter (the real part, *n*). The RI values of SOA derived from long-chain alkanes are investigated in various studies, as shown in **Table 5**. According to the available studies, the SOA derived from long-chain alkanes has negligible absorption at the wavelength of 375 and 532 nm (Li et al., 2020b) and over the visible range between 400 and 700 nm (Updyke et al., 2012). Therefore, only the real parts of the RI are listed in Table 5. Due to the various reaction conditions, the chemical composition of SOA generated from the same precursor is different, resulting in different optical properties. Li et al. (2017) reported the RI values of SOA derived from *n*-dodecane, *n*-pentadecane, and *n*-heptadecane under various conditions and found that both the NO_x concentration and inorganic aerosol seeds can affect the chemical compositions of the formed SOA and the scattering properties of the SOA at 532 nm. As mentioned above, the environmental temperature could also influence the reaction pathways of the long-chain alkanes, and the scattering properties of SOA derived from C_{12} alkanes at 532 and 375 nm are both enhanced under 5°C compared to that under 25°C (Li et al., 2020b).

Density is also an important parameter of SOA. Li et al. (2020b) reported a density of 1.1 g/cm^3 for the n-dodecane SOA generated under low-NO_x conditions, using a scanning mobility particle sizer (SMPS) and a centrifugal particle mass analyzer (CPMA). Lim and Ziemann (2009b) measured the density of n-hexadecane SOA (in the presence of NO_x) to be 1.06 g/cm^3 with a microliter syringe and a mass balance. Loza et al. (2014) calculated the SOA density by comparing the SOA diameter measured by the AMS (D_{va}, the mean vacuum aerodynamic diameter) to that measured by the DMA (D_m, the electric mobility diameter), $\rho = D_{va}/D_m$. The reported density of C_{12} SOA density is: (1) under low-NO_x condition, 1.12±0.03 g/cm^3 for *n*-dodecane, 1.12±0.03 g/cm^3 for 2-methylundecane, 1.17±0.03 g/cm^3 for hexylcyclohexane, and 1.28±0.03 g/cm^3 for cyclododecane; (2) under high-NO_x condition, 1.28±0.01 g/cm^3 for *n*-dodecane, 1.28±0.01 g/cm^3 for 2-methylundecane, 1.29±0.01 g/cm^3 for hexylcyclohexane, and 1.23±0.02 g/cm^3 for cyclododecane. In general, the SOA densities derived from alkanes under various conditions are in the range of 1-1.4 g/cm^3.

4. Model simulation

Atmospheric model is an important tool for integrating the atmospheric chemistry of the long-chain alkanes with that

Table 5 – RI values (real part) for SOA from long-chain alkanes as measured in various studies

Precursors	Oxidation Pathway	Techniques	Temperature (°C)	λ (nm)	RI values (*n*)	References
***n*-Dodecane**	H_2O_2	CRDs + PAX + 5 m^3 Teflon smog chamber	25	532	$1.482^{+0.004}_{-0.01}$	Li et al., 2020b
				375	$1.520^{+0.01}_{-0.01}$	
			5	532	$1.515^{+0.011}_{-0.013}$	
				375	$1.542^{+0.018}_{-0.01}$	
	H_2O_2	CRDs + 5 m^3 Teflon smog chamber	25	532	1.484	Li et al., 2017
	H_2O_2 + seed				1.466	
	HONO				1.414	
	HONO + seed				1.501	
***n*-Pentadecane**	H_2O_2	CRDs + 5 m^3 Teflon smog chamber	25	532	1.484	
	H_2O_2 + seed				1.438	
	HONO				1.457	
	HONO + seed				1.476	
***n*-Heptadecane**	H_2O_2	CRDs + 5 m^3 Teflon smog chamber	25	532	1.478	
	H_2O_2 + seed				1.45	
	HONO				1.435	
	HONO + seed				1.471	
2-Methylundecane	H_2O_2	CRDs + 5 m^3 Teflon smog chamber	25	532	1.482-1.483	Li et al., 2021
			5	532	1.515-1.516	
Hexylcyclohexane	H_2O_2		25	532	1.459-1.462	
			5	532	1.489-1.492	
Cyclododecane	H_2O_2		25	532	1.450-1.451	
			5	532	1.485-1.487	

of other important processes, such as emissions, transport, dispersion, and deposition. The air quality models can simulate concentrations of air pollutants with a high time resolution at global or regional scales. Based on the semi-empirical parameterization scheme, the two product (2P) model (Odum et al., 1996) and the volatility basis set (VBS) approach (Donahue et al., 2006) are established for improving the model performance of SOA formation.

According to previous studies, there are discrepancies between model simulation and field observation for SOA formation. In the ambient air, reactive anthropogenic VOCs (AVOCs) can produce much larger amounts of SOA than model prediction (Volkamer et al., 2006). The discrepancies between model and observation may come from the incomplete understanding of the chemical mechanism (Shrivastava et al., 2017), and/or there may be unknown sources that are not included in the model simulations (Yang et al., 2019). The gap between observation and model simulation has attracted attention to add new mechanisms or sources to the model.

Long-chain alkanes, as a representative substance of intermediate volatile organic compounds (IVOCs) (Robinson et al., 2007), are often ignored in field observations and model simulations. However, due to its high contribution to secondary organic aerosols (Gentner et al., 2012; Zhao et al., 2014), long-chain alkanes have begun to be considered in model simulations in the last decade. Thus, the following studies below mainly include the model simulations related to long-chain alkanes' SOA mass concentration and yields.

In earlier studies, scholars have begun to study the contribution of long-chain alkanes to SOA in the atmosphere. Hodzic et al. (2010) applied the 3-D regional air quality model CHIMERE to estimate the potential contributions of intermediate volatility organic compounds (IVOCs) and semi-volatile organic compounds (SVOCs) to SOA formation in the 2006 field observation in and around Mexico City. The volatility distribution of primary organic aerosols (POA), gas-phase oxidation of their vapors, and related gas-particle distributions were included in the model. They found that the predicted SOA concentration had a substantial enhancement compared to the results that the S/IVOCs were not considered (Hodzic et al., 2009). The gap between oxygenated organic aerosol (OOA) observations and simulations had been reduced substantially: with the initially proposed volatility distribution and aging mechanisms of SVOCs by Robinson et al. (2007), the average SOA concentration increased about 3.8 $\mu g/m^3$ (a factor of 2.5); with the updated mechanisms by Grieshop et al. (2009), the average SOA concentration increased about 8.7 $\mu g/m^3$ (a factor of 4). Lee-Taylor et al. (2011) investigated the evolution of organic aerosols in Mexico City and its outflow plume with the gas phase photochemistry model generator of explicit chemistry and kinetics of organics in the atmosphere (GECKO-A). A chemical box model was used to determine the vapor pressures and the gas-particle partitioning process of the formed intermediate products. The simulation results were compared to the MILAGRO observations made in March 2006, and successfully reproduced the diurnal variation for both POA and SOA. In this simulation work, larger *n*-alkanes (C_{11} to C_{25}) were considered as precursors, which were used as surrogates for hydrocarbons with similar volatility. Simulation results indicated that ≥75% of the SOA were derived from the larger *n*-alkanes. Pye and Pouliot (2012) simulated the aerosol formation from primary precursors with the Community Multiscale Air Quality (CMAQ) model version 5.0. In addition to the conventional SOA sources (e.g., aromatics, monoterpenes, sesquiterpenes, isoprene, aqueous processes that could produce aerosols), alkanes and polycyclic aromatic hydrocarbons (PAHs) were included in this model. Simulation results showed that compared to PAHs, alkanes could generate more SOA due

to their relatively higher emissions. Compared to the traditional SOA sources, although the concentrations of alkanes and PAHs in the atmosphere were not high, their contribution to SOA could not be ignored. All the results above highlight the importance of lower volatile organic compounds to SOA in the atmosphere, e.g., long-chain alkanes.

In recent years, scholars in China have also begun to pay attention to and carry out research related to the lower volatile organic compounds, e.g., IVOCs, SVOCs, *n*-dodecane. Zhao et al. (2016) developed the CMAQ/2D-VBS model to quantify the effect of organic aerosol aging and IVOCs emissions on aerosol pollutions in China. 2D-VBS parameters were determined by performing a series of smog chamber experiments related to SOA formation, the parameters were then applied in the three-dimensional chemical transport models (3D-CTMs). They found that the discrepancies between observation and simulation reduced significantly after considering the organic aerosol aging and IVOC emissions: the IVOCs emissions could increase the OA and SOA concentrations in Eastern China by a factor of 10, and the OA aging could increase the OA and SOA concentrations by about 40%. Yang et al. (2019) applied a 3D regional atmospheric CTM, nested air quality prediction modeling system (NAQPMS), to simulate the SOA concentrations in central and eastern China in 2014. SOA mass yields of n-dodecane obtained with smog chamber were used to generate VBS parameters for the model. Results showed that after considering the contribution of alkanes, the SOA concentration increased by 10–20 $\mu g/m^3$ in winter compared to the base scenario, which significantly reduced the discrepancy between observations and simulations. In this work, n-dodecane was taken as the representative of IVOCs; to understand the SOA formation more thoroughly in the atmosphere, it is necessary to conduct further research on IVOCs parameterization.

Li et al. (2020a) investigated the organic aerosols distribution and evolution in the Beijing-Tianjin-Hebei region during the 2014 winter with a regional air quality model system (RAQMS), considering the emission inventories and SOA formation of S/IVOCs. They found that the contributions to SOA formation of SVOCs and IVOCs were 40.1% and 9.4%, respectively, indicating the important role of S/IVOCs in SOA formation in China. Li et al. (2020a) also expressed the observation urgency of S/IVOCs emissions from anthropogenic sources in China. Yao et al. (2020) simulated the SOAs formation over the Pearl River Delta (PRD) region in China with the comprehensive air quality model with extensions (CAMx). Results showed that the oxidation of S/IVOCs could contribute 4-7 $\mu g/m^3$ to SOA concentration in the center of the PRD region, and contribute 1-2 $\mu g/m^3$ to SOA concentration in the rural sites of the PRD region. While the observed SOA concentration was approximately 1-7 $\mu g/m^3$, the results implied that the IVOCs/SVOCs emission were important to atmospheric SOA concentration.

As mentioned in the above literature, when S/IVOCs sources such as long-chain alkanes are considered in the model simulations, the gap between model simulation and field observation is reduced. For atmospheric concentrations of IVOCs (e.g., long-chain alkanes), the data obtained by field observations is still relatively limited; the field observations related to long-chain alkanes should be strengthened. Meanwhile, long-chain alkanes have a higher contribution to the formation of SOA, the reaction pathways of which should be considered in the model. Further experiments about the chemical mechanism and SOA yields of long-chain alkanes under various oxidation conditions are necessary for the laboratory, to make the obtained parameters meet the demand for increased accuracy of model simulation.

5. Summary and perspectives

As representative substances of intermediate volatile organic compounds (IVOCs), long-chain alkanes have been proposed to be an important potential source of secondary organic aerosols in the atmosphere. This work briefly summarizes the detection methods, field observations, and model simulations of long-chain alkanes in Section 1, 2 and 4, and summarizes the laboratory research of long-chain alkanes in detail in Section 3.

Detection Methods: With the development of technology, the accuracy and time resolution of related techniques have been improved. However, due to the complexity of long-chain alkane types (such as isomers), it is difficult to distinguish them from existing equipment. Therefore, equipment with high resolution and time resolution is required to satisfy field observations for complex environments.

Field observations: With the increasing recognition of measurements related to long-chain alkanes, researchers have learned much about long-chain alkanes in the atmosphere. The anthropogenic sources of long-chain alkanes mainly include fossil fuels and volatile chemical products; the biological sources mainly include animal husbandry, plants, microbe, and combustion of biomass. In urban areas, vehicle emissions are one of the important contributors to long-chain alkanes.

The concentration of long-chain alkanes in both the particles and gas phase varies due to different sampling locations, sampling methods, and detection methods, as shown in **Table 1**. However, the overall results show that the concentration of long-chain alkanes in the atmosphere cannot be ignored, especially in the gas phase. The monitoring of long-chain alkane species should be strengthened in field observations. Considering the reaction activity of long-chain alkanes with OH radicals, observation sites related to long-chain alkanes should not only be located near urban emission points but also located in downwind suburban environments.

Laboratory studies: Laboratory research on long-chain alkanes is still very scarce. Halogens are one of the important oxidants in the atmospheric environment, but there are very few studies on their kinetics with long-chain alkanes. The reaction mechanism and SOA yields of long-chain alkanes under different conditions are different, such as the influence of temperature, relative humidity, oxidant types, oxidant concentration, seed, etc., and further research is needed in this area. Future studies should include the reactions under various environmental factors to better understand the specific reaction mechanisms. Besides, according to the existing studies, there is limited research on the optical properties of SOA derived from long-chain alkanes, and thus optical properties of SOA derived from long-chain alkanes with different carbon numbers or different chemical structures under various conditions need to be investigated in the future studies.

Besides, the existing research is mostly about the reaction system of single long-chain alkanes, and the oxidation process of long-chain alkanes with other coexisting VOCs is rarely studied.

Model simulations: As the relatively high SOA formation potential of long-chain alkanes, they should be explicitly included in the current model simulation for SOA formation. When long-chain alkanes are added to the model simulations, the discrepancies between field observations and model simulations for SOA formation generally decrease. However, the parameters added to the model are still not fully representative for various precursors. Specific parameters input is required for model simulations related to specific regions under different conditions.

Overall, the field observation of long-chain alkanes in both the gas and particle phase in specific areas should be strengthened, and more experiments should be carried out in the laboratory according to the parameter requirements of the model to achieve further improvement of the model simulation accuracy and forecast accuracy.

Acknowledgments

This work was supported by the Postdoctoral Research Foundation of China (No. 2019M660752), Beijing Municipal Commission of Education (No. Z181100005418015), and the National Natural Science Foundation of China (Nos. 91744204, 41822703).

Appendix A Supplementary data

Supplementary data associated with this article can be found in the online version at doi:10.1016/j.jes.2021.07.021.

REFERENCES

Agrawal, H., Sawant, A.A., Jansen, K., Miller, J.W., Cocker, D.R., 2008. Characterization of chemical and particulate emissions from aircraft engines. Atmos. Environ. 42, 4380–4392.

Aimanant, S., Ziemann, P.J., 2013. Chemical mechanisms of aging of aerosol formed from the reaction of n-pentadecane with OH radicals in the presence of NOx. Aerosol Sci. Technol. 47, 979–990.

Ait-Helal, W., Borbon, A., Sauvage, S., de Gouw, J.A., Colomb, A., Gros, V., et al., 2014. Volatile and intermediate volatility organic compounds in suburban Paris: variability, origin and importance for SOA formation. Atmos. Chem. Phys. 14, 10439–10464.

Amador Muñoz, O., Misztal, P.K., Weber, R., Worton, D.R., Zhang, H., Drozd, G., et al., 2016. Sensitive detection of n-alkanes using a mixed ionization mode Proton-Transfer Reaction-Mass Spectrometer. Atmos. Meas. Techn. 9, 5315–5329.

Aschmann, S.M., Atkinson, R., 1995. Rate constants for the gas-phase reactions of alkanes with Cl atoms at 296 ± 2 K. Inter. J. Chem. Kinet. 27, 613–622.

Atkinson, R., 1990. Gas-phase tropospheric chemistry of organic-compounds: A review. Atmos. Environ. Part A-Gen. Top. 24, 1–41.

Atkinson, R., 1997. Gas-phase tropospheric chemistry of volatile organic compounds: 1. alkanes and alkenes. J. Phys. Chem. Ref. Data 26, 215.

Atkinson, R., 2000. Atmospheric chemistry of VOCs and NOx. Atmos. Environ. 34, 2063–2101.

Atkinson, R., 2003. Kinetics of the gas-phase reactions of OH radicals with alkanes and cycloalkanes. Atmos. Chem. Phys. 3, 2233–2307.

Atkinson, R., Arey, J., 2003. Atmospheric degradation of volatile organic compounds. Chem. Rev. 103, 4605–4638.

Behnke, W., Hollander, W., Koch, W., Nolting, F., Zetzsch, C., 1988. A smog chamber for studies of the photochemical degradation of chemicals in the presence of aerosols. Atmos. Environ. 22, 1113–1120.

Bejan, I.G., Winiberg, F.A.F., Mortimer, N., Medeiros, D.J., Brumby, C.A., Orr, S.C., et al., 2018. Gas-phase rate coefficients for a series of alkyl cyclohexanes with OH radicals and Cl atoms. Inter. J. Chem. Kinet. 50, 544–555.

Bianchi, F., Kurten, T., Riva, M., Mohr, C., Rissanen, M.P., Roldin, P., et al., 2019. Highly oxygenated organic molecules (HOM) from gas-phase autoxidation involving peroxy radicals: A key contributor to atmospheric aerosol. Chem. Rev. 119, 3472–3509.

Bray, E.E., Evans, E.D., 1961. Distribution of normal-paraffins as a clue to recognition of source beds. Geochim. Cosmochim. Acta 22, 2–15.

Cao, G., Jang, M., 2007. Effects of particle acidity and UV light on secondary organic aerosol formation from oxidation of aromatics in the absence of NOx. Atmos. Environ. 41, 7603–7613.

Carter, W. P. L., 2000. Documentation of the SAPRC-99 chemical mechanism for VOC reactivity assessment. Report to the California Air Resources Board Contracts 92-329 and 95-308.

Carter, W. P. L., Luo, D., Malkina, I. L., 2002. Investigation of the ozone formation potentials of selected branched alkanes and mineral spirits samples. Report to Safety-Kleen Corporation.

Cartier, W.P.L., Atkinson, R., 1985. Atmospheric chemistry of alkanes. J. Atmos. Chem. 3, 377–405.

Chan, A.W.H., Isaacman, G., Wilson, K.R., Worton, D.R., Ruehl, C.R., Nah, T., et al., 2013. Detailed chemical characterization of unresolved complex mixtures in atmospheric organics: Insights into emission sources, atmospheric processing, and secondary organic aerosol formation. J. Geophys. Res. Atmos. 118, 6783–6796.

Charron, A., Polo-Rehn, L., Besombes, J.L., Golly, B., Buisson, C., Chanut, H., et al., 2019. Identification and quantification of particulate tracers of exhaust and non-exhaust vehicle emissions. Atmos. Chem. Phys. 19, 5187–5207.

de Gouw, J., Warneke, C., 2007. Measurements of volatile organic compounds in the earths atmosphere using proton-transfer-reaction mass spectrometry. Mass Spectr. Rev. 26, 223–257.

de Gouw, J.A., Middlebrook, A.M., Warneke, C., Ahmadov, R., Atlas, E.L., Bahreini, R., et al., 2011. Organic aerosol formation downwind from the deepwater horizon oil spill. Science 331, 1295–1299.

Deng, W., Hu, Q., Liu, T., Wang, X., Zhang, Y., Song, W., et al., 2017. Primary particulate emissions and secondary organic aerosol (SOA) formation from idling diesel vehicle exhaust in China. Sci. Total Environ. 593-594, 462–469.

Dominici, F., Peng, R.D., Bell, M.L., Pham, L., McDermott, A., Zeger, S.L., et al., 2006. Fine particulate air pollution and hospital admission for cardiovascular and respiratory diseases. JAMA-J. Am. Med. Assoc. 295, 1127–1134.

Donahue, N.M., Kroll, J.H., Pandis, S.N., Robinson, A.L., 2012. A two-dimensional volatility basis set – Part 2: Diagnostics of organic-aerosol evolution. Atmos. Chem. Phys. 12, 615–634.

Donahue, N.M., Robinson, A.L., Stanier, C.O., Pandis, S.N., 2006. Coupled partitioning, dilution, and chemical aging of semivolatile organics. Environ. Sci. Technol. 40, 2635–2643.

Duan, F., He, K., Liu, X., 2010. Characteristics and source identification of fine particulate n-alkanes in Beijing, China. J. Environ. Sci. 22, 998–1005.
Erickson, M.H., Gueneron, M., Jobson, B.T., 2014. Measuring long chain alkanes in diesel engine exhaust by thermal desorption PTR-MS. Atmos. Meas. Tech. 7, 225–239.
Fahnestock, K.A.S., Yee, L.D., Loza, C.L., Coggon, M.M., Schwantes, R., Zhang, X., et al., 2015. Secondary organic aerosol composition from C_{12} alkanes. J. Phys. Chem. A 119, 4281–4297.
Gentner, D.R., Isaacman, G., Worton, D.R., Chan, A.W.H., Dallmann, T.R., Davis, L., et al., 2012. Elucidating secondary organic aerosol from diesel and gasoline vehicles through detailed characterization of organic carbon emissions. P. Natl. Acad. Sci. USA 109, 18318–18323.
Gentner, D.R., Jathar, S.H., Gordon, T.D., Bahreini, R., Day, D.A., El Haddad, I., et al., 2017. Review of urban secondary organic aerosol formation from gasoline and diesel motor vehicle emissions. Environ. Sci. Technol. 51, 1074–1093.
Goldstein, A.H., Galbally, I.E., 2007. Known and unexplored organic constituents in the Earth's atmosphere. Environ. Sci. Technol. 41, 1514–1521.
Graus, M., Mueller, M., Hansel, A., 2010. High resolution PTR-TOF: Quantification and formula confirmation of VOC in real time. J. Am. Soc. Mass Spectr. 21, 1037–1044.
Grieshop, A.P., Logue, J.M., Donahue, N.M., Robinson, A.L., 2009. Laboratory investigation of photochemical oxidation of organic aerosol from wood fires 1: measurement and simulation of organic aerosol evolution. Atmos. Chem. Phys. 9, 1263–1277.
Gueneron, M., Erickson, M.H., VanderSchelden, G.S., Jobson, B.T., 2015. PTR-MS fragmentation patterns of gasoline hydrocarbons. Inter. J. Mass Spectrom. 379, 97–109.
Hallquist, M., Wenger, J.C., Baltensperger, U., Rudich, Y., Simpson, D., Claeys, M., et al., 2009. The formation, properties and impact of secondary organic aerosol: current and emerging issues. Atmos. Chem. Phys. 9, 5155–5236.
He, L.Y., Hu, M., Zhang, Y.H., Huang, X.F., Yao, T.T., 2008. Fine particle emissions from on-road vehicles in the Zhujiang Tunnel, China. Environ. Sci. Technol. 42, 4461–4466.
Hodzic, A., Jimenez, J.L., Madronich, S., Aiken, A.C., Bessagnet, B., Curci, G., et al., 2009. Modeling organic aerosols during MILAGRO: importance of biogenic secondary organic aerosols. Atmos. Chem. Phys. 9, 6949–6981.
Hodzic, A., Jimenez, J.L., Madronich, S., Canagaratna, M.R., DeCarlo, P.F., Kleinman, L., et al., 2010. Modeling organic aerosols in a megacity: potential contribution of semi-volatile and intermediate volatility primary organic compounds to secondary organic aerosol formation. Atmos. Chem. Phys. 10, 5491–5514.
Huang, C., Hu, Q.Y., Li, Y.J., Tian, J.J., Ma, Y.G., Zhao, Y.L., et al., 2018. Intermediate volatility organic compound emissions from a large cargo vessel operated under real-world conditions. Environ. Sci. Technol. 52, 12934–12942.
Hunter, J.F., Carrasquillo, A.J., Daumit, K.E., Kroll, J.H., 2014. Secondary organic aerosol formation from acyclic, monocyclic, and polycyclic alkanes. Environ. Sci. Technol. 48, 10227–10234.
Calvert, J.G., Derwent, R.G., Orlando, J.J., Tyndall, G.S., Wallington, T.J., 2008. Mechanisms of atmospheric oxidation of the alkanes. Oxford University Press, New York.
Jang, M.S., Czoschke, N.M., Lee, S., Kamens, R.M., 2002. Heterogeneous atmospheric aerosol production by acid-catalyzed particle-phase reactions. Science 298, 814–817.
Jathar, S.H., Friedman, B., Galang, A.A., Link, M.F., Brophy, P., Volckens, J., et al., 2017. Linking load, fuel, and emission controls to photochemical production of secondary organic aerosol from a diesel engine. Environ. Sci. Technol. 51, 1377–1386.
Jones, A., Harrison, R., 2006. Estimation of the emission factors of particle number and mass fractions from traffic at a site where mean vehicle speeds vary over short distances. Atmos. Environ. 40, 7125–7137.
Jordan, A., Haidacher, S., Hanel, G., Hartungen, E., Herbig, J., Maerk, L., et al., 2009. An online ultra-high sensitivity Proton-transfer-reaction mass-spectrometer combined with switchable reagent ion capability (PTR+SRI-MS). Int. J. Mass Spectrom. 286, 32–38.
Kang, M.J., Ren, L.J., Ren, H., Zhao, Y., Kawamura, K., Zhang, H.L., et al., 2018. Primary biogenic and anthropogenic sources of organic aerosols in Beijing, China: Insights from saccharides and n-alkanes. Environ. Pollut. 243, 1579–1587.
Koss, A.R., Warneke, C., Yuan, B., Coggon, M.M., Veres, P .R., de Gouw, J.A., 2016. Evaluation of NO^+ reagent ion chemistry for online measurements of atmospheric volatile organic compounds. Atmos. Meas. Techn. 9, 2909–2925.
Lambe, A.T., Onasch, T.B., Croasdale, D.R., Wright, J.P., Martin, A.T., Franklin, J.P., et al., 2012. Transitions from functionalization to fragmentation reactions of laboratory secondary organic aerosol (SOA) generated from the OH oxidation of alkane precursors. Environ. Sci. Technol. 46, 5430–5437.
Lamkaddam, H., Gratien, A., Pangui, E., Cazaunau, M., Picquet-Varrault, B., Doussin, J.F., 2016. High-NOx photooxidation of n-dodecane: Temperature dependence of SOA formation. Environ. Sci. Technol. 51, 192–201.
Lamkaddam, H., Gratien, A., Pangui, E., David, M., Peinado, F., Polienor, J.M, et al., 2020. Role of relative humidity in the secondary organic aerosol formation from high-NOx photooxidation of long-chain alkanes: n-Dodecane case study. ACS Earth Space Chem. 4, 2414–2425.
Lamkaddam, H., Gratien, A., Ropion, M., Pangui, E., Doussin, J.F., 2019. Kinetic study of the temperature dependence of OH-initiated oxidation of n-dodecane. J. Phys. Chem. A 123, 9462–9468.
Lee-Taylor, J., Madronich, S., Aumont, B., Baker, A., Camredon, M., Hodzic, A., et al., 2011. Explicit modeling of organic chemistry and secondary organic aerosol partitioning for Mexico City and its outflow plume. Atmos. Chem. Phys. 11, 13219–13241.
Li, H., Li, H., Lu, J., Feng, J., Yu, Y., Xia, F., et al., 2015. Distribution characteristics and source identification of n-alkanes in $PM_{2.5}$ in typical urban area of Beijing. Res. Environ. Sci. 28, 691–696.
Li, J., Han, Z.W., Li, J.W., Liu, R.T., Wu, Y.F., Liang, L., et al., 2020a. The formation and evolution of secondary organic aerosol during haze events in Beijing in wintertime. Sci. Total Environ. 703, 16.
Li, J., Li, K., Wang, W., Wang, J., Peng, C., Ge, M., 2017. Optical properties of secondary organic aerosols derived from long-chain alkanes under various NOx and seed conditions. Sci. Total Environ. 579, 1699–1705.
Li, J., Wang, W., Li, K., Zhang, W., Peng, C., Liu, M., et al., 2021. Effect of chemical structure on optical properties of secondary organic aerosols derived from C_{12} alkanes. Sci. Total Environ. 751, 141620.
Li, J., Wang, W., Li, K., Zhang, W., Peng, C., Zhou, L., et al., 2020b. Temperature effects on optical properties and chemical composition of secondary organic aerosol derived from n-dodecane. Atmos. Chem. Phys. 20, 8123–8137.
Li, K., Liggio, J., Han, C., Liu, Q., Moussa, S.G., Lee, P., et al., 2019a. Understanding the impact of high-NOx conditions on the formation of secondary organic aerosol in the photooxidation of oil sand-related precursors. Environ. Sci. Technol. 53, 14420–14429.
Li, K., Liggio, J., Lee, P., Han, C., Liu, Q., Li, S.M., 2019b. Secondary organic aerosol formation from α-pinene, alkanes, and

oil-sands-related precursors in a new oxidation flow reactor. Atmos. Chem. Phys. 19, 9715–9731.
Li, Y., Cao, J., Li, J., Zhou, J., Xu, H., Zhang, R., et al., 2013. Molecular distribution and seasonal variation of hydrocarbons in $PM_{2.5}$ from Beijing during 2006. Particuology 11, 78–85.
Liggio, J., Li, S.M., Hayden, K., Taha, Y.M., Stroud, C., Darlington, A., et al., 2016. Oil sands operations as a large source of secondary organic aerosols. Nature 534 (7605), 91.
Lim, Y.B., Ziemann, P.J., 2005. Products and mechanism of secondary organic aerosol formation from reactions of n-alkanes with OH radicals in the presence of NOx. Environ. Sci. Technol. 39, 9229–9236.
Lim, Y.B., Ziemann, P.J., 2009a. Chemistry of secondary organic aerosol formation from OH radical-initiated reactions of linear, branched, and cyclic alkanes in the presence of NOx. Aerosol Sci. Technol. 43, 604–619.
Lim, Y.B., Ziemann, P.J., 2009b. Effects of molecular structure on aerosol yields from OH radical-initiated reactions of linear, branched, and cyclic alkanes in the presence of NOx. Environ. Sci. Technol. 43, 2328–2334.
Liu, H., Man, H., Cui, H., Wang, Y., Deng, F., Wang, Y., et al., 2017. An updated emission inventory of vehicular VOCs and IVOCs in China. Atmos. Chem. Phys. 17, 12709–12724.
Lou, H.J., Hao, Y.J., Zhang, W.W., Su, P.H., Zhang, F., Chen, Y.J., et al., 2019. Emission of intermediate volatility organic compounds from a ship main engine burning heavy fuel oil. J. Environ. Sci. 84, 197–204.
Loza, C.L., Craven, J.S., Yee, L.D., Coggon, M.M., Schwantes, R.H., Shiraiwa, M., et al., 2014. Secondary organic aerosol yields of 12-carbon alkanes. Atmos. Chem. Phys. 14, 1423–1439.
Luo, H., Jia, L., Wan, Q., An, T., Wang, Y., 2019. Role of liquid water in the formation of O_3 and SOA particles from 1,2,3-trimethylbenzene. Atmos. Environ. 217, 116955.
Ma, H., Li, Y., Qian, F., Xiao, L., He, X., 2013. Pollution characteristics of n-alkane in aerosol particles of Beijing. Environ. Sci. Technol. 36, 50–54.
Ma, P., Zhang, P., Shu, J., Yang, B., Zhang, H., 2018. Characterization of secondary organic aerosol from photo-oxidation of gasoline exhaust and specific sources of major components. Environ. Pollut. 232, 65–72.
Martin, P., Tuazon, E.C., Aschmann, S.M., Arey, J., Atkinson, R., 2002. Formation and atmospheric reactions of 4,5-dihydro-2-methylfuran. J. Phys. Chem. A 106, 11492–11501.
Nolting, F., Behnke, W., Zetzsch, C., 1988. A smog chamber for studies of the reactions of terpenes and alkanes with ozone and OH. J. Atmos. Chem. 6, 47–59.
Odum, J.R., Hoffmann, T., Bowman, F., Collins, D, Flagan, R.C., Seinfeld, J.H., 1996. Gas/particle partitioning and secondary organic aerosol yields. Environ. Sci. Technol. 30, 2580–2585.
Pandis, S.N., Donahue, N.M., Murphy, B.N., Riipinen, I., Fountoukis, C., Karnezi, E., et al., 2013. Introductory lecture: Atmospheric organic aerosols: insights from the combination of measurements and chemical transport models. Faraday Discuss. 165, 9–24.
Perrone, M.G., Carbone, C., Faedo, D., Ferrero, L., Maggioni, A., Sangiorgi, G., et al., 2014. Exhaust emissions of polycyclic aromatic hydrocarbons, n-alkanes and phenols from vehicles coming within different European classes. Atmos. Environ. 82, 391–400.
Pierson, W.R., Gertler, A.W., Robinson, N.F., Sagebiel, J.C., Zielinska, B., Bishop, G.A., et al., 1996. Real-world automotive emissions: Summary of studies in the Fort McHenry and Tuscarora Mountain Tunnels. Atmos. Environ. 30, 2233–2256.
Presto, A.A., Miracolo, M.A., Donahue, N.M., Robinson, A.L., 2010. Secondary organic aerosol formation from high-NOx photo-oxidation of low volatility precursors: n-Alkanes. Environ. Sci. Technol. 44, 2029–2034.
Pye, H.O., Pouliot, G.A., 2012. Modeling the role of alkanes, polycyclic aromatic hydrocarbons, and their oligomers in secondary organic aerosol formation. Environ. Sci. Technol. 46, 6041–6047.
Qi, L., Liu, H., Shen, X., Fu, M., Huang, F., Man, H., et al., 2019. Intermediate-volatility organic compound emissions from nonroad construction machinery under different operation modes. Environ. Sci. Technol. 53, 13832–13840.
Requia, W.J., Higgins, C.D., Adams, M.D., Mohamed, M., Koutrakis, P., 2018. The health impacts of weekday traffic: A health risk assessment of $PM_{2.5}$ emissions during congested periods. Environ. Int. 111, 164–176.
Robinson, A.L., Donahue, N.M., Shrivastava, M.K., Weitkamp, E.A., Sage, A.M., Grieshop, A .P., et al., 2007. Rethinking organic aerosols: Semivolatile emissions and photochemical aging. Science 315, 1259–1262.
Schauer, J.J., Kleeman, M.J., Cass, G.R., Simoneit, B.R.T., 1999. Measurement of emissions from air pollution sources. 2. C_1 through C_{30} organic compounds from medium duty diesel trucks. Environ. Sci. Technol. 33, 1578–1587.
Schauer, J.J., Kleeman, M.J., Cass, G.R., Simoneit, B.R.T., 2002. Measurement of emissions from air pollution sources. 5. C_1-C_{32} organic compounds from gasoline-powered motor vehicles. Environ. Sci. Technol. 36, 1169–1180.
Schnelle-Kreis, J., Sklorz, M., Orasche, J., Stoelzel, M., Peters, A., Zimmermann, R., 2007. Semi-volatile organic compounds in ambient $PM_{2.5}$. Seasonal trends and daily resolved source contributions. Environ. Sci. Technol. 41, 3821–3828.
Shi, B., Wang, W., Zhou, L., Li, J., Wang, J., Chen, Y., et al., 2019a. Kinetics and mechanisms of the gas-phase reactions of OH radicals with three C_{15} alkanes. Atmos. Environ. 207, 75–81.
Shi, B., Wang, W., Zhou, L., Sun, Z., Fan, C., Chen, Y., et al., 2019b. Atmospheric oxidation of $C_{10\sim14}$ n-alkanes initiated by Cl atoms: Kinetics and mechanism. Atmos. Environ. 222, 117166.
Shrivastava, M., Cappa, C.D., Fan, J., Goldstein, A.H., Guenther, A.B., Jimenez, J.L., et al., 2017. Recent advances in understanding secondary organic aerosol: Implications for global climate forcing. Rev. Geophys. 55, 509–559.
Siegl, W.O., Hammerle, R.H., Herrmann, H.M., Wenclawiak, B.W., Luers-Jongen, B., 1999. Organic emissions profile for a light-duty diesel vehicle. Atmos. Environ. 33, 797–805.
Simoneit, B.R.T., 2002. Biomass burning - A review of organic tracers for smoke from incomplete combustion. Appl. Geochem. 17, 129–162.
Simoneit, B.R.T., Mazurek, M.A., 1982. Organic-matter of the troposphere 2: Natural background of biogenic lipid matter in aerosols over the rural western united states. Atmos. Environ. 16, 2139–2159.
Sivaramakrishnan, R., Michael, J.V., 2009. Rate constants for OH with selected large alkanes: Shock-tube measurements and an improved group scheme. J. Phys. Chem. A 113, 5047–5060.
Sulzer, P., Hartungen, E., Hanel, G., Feil, S., Winkler, K., Mutschlechner, P., et al., 2014. A proton transfer reaction-quadrupole interface time-of-flight mass spectrometer (PTR-Qi-TOF): High speed due to extreme sensitivity. Int. J. Mass Spectrom. 368, 1–5.
Tkacik, D.S., Presto, A.A., Donahue, N.M., Robinson, A.L., 2012. Secondary organic aerosol formation from intermediate-volatility organic compounds: Cyclic, linear, and branched alkanes. Environ. Sci. Technol. 46, 8773–8781.
Tobias, H.J., Docherty, K.S., Beving, D.E., Ziemann, P.J., 2000. Effect of relative humidity on the chemical composition of secondary organic aerosol formed from reactions of 1-tetradecene and O_3. Environ. Sci. Technol. 34, 2116–2125.
Updyke, K.M., Nguyen, T.B., Nizkorodov, S.A., 2012. Formation of brown carbon via reactions of ammonia with secondary organic aerosols from biogenic and anthropogenic precursors. Atmos. Environ. 63, 22–31.
Volkamer, R., Jimenez, J.L., San Martini, F., Dzepina, K., Zhang, Q., Salcedo, D., et al., 2006. Secondary organic aerosol formation

from anthropogenic air pollution: Rapid and higher than expected. Geophys. Res. Lett. 33, 4.
Wang, C., Yuan, B., Wu, C., Wang, S., Qi, J., Wang, B., et al., 2020a. Measurements of higher alkanes using NO^+ chemical ionization in PTR-ToF-MS: important contributions of higher alkanes to secondary organic aerosols in China. Atmos. Chem. Phys. 20, 14123–14138.
Wang, D.S., Hildebrandt Ruiz, L., 2018. Chlorine-initiated oxidation of n-alkanes under high-NOx conditions: insights into secondary organic aerosol composition and volatility using a FIGAERO–CIMS. Atmos. Chem. Phys. 18, 15535–15553.
Wang, Q., Huang, L., Wang, Y.J., Yin, S.J., Zhang, Q., Yi, X., et al., 2020b. Emission inventory of intermediate volatility organic compounds from vehicles in the Yangtze River Delta in 2017 and the impact on the formation potential of secondary organic aerosols. Environ. Sci. 41, 125–132.
Wu, L., Wang, X., Lu, S., Shao, M., Ling, Z., 2019. Emission inventory of semi-volatile and intermediate-volatility organic compounds and their effects on secondary organic aerosol over the Pearl River Delta region. Atmos. Chem. Phys. 19, 8141–8161.
Wu, R., Xie, S., 2018. Spatial distribution of secondary organic aerosol formation potential in China derived from speciated anthropogenic volatile organic compound emissions. Environ. Sci. Technol. 52, 8146–8156.
Xu, R., Alam, M.S., Stark, C., Harrison, R.M., 2020. Composition and emission factors of traffic- emitted intermediate volatility and semi-volatile hydrocarbons (C_{10}–C_{36}) at a street canyon and urban background sites in central London, UK. Atmos. Environ. 231, 117448.
Yang, W., Li, J., Wang, W., Li, J., Ge, M., Sun, Y., et al., 2019. Investigating secondary organic aerosol formation pathways in China during 2014. Atmos. Environ. 213, 133–147.
Yao, L., Li, X.R., Guo, X.Q., Liu, X.R., Wang, Y.S., 2009. Pollution characteristics of n-alkanes in atmospheric fine particles during Spring Festival of 2007 in Beijing. Environ. Sci. 30, 589–593.
Yao, T., Li, Y., Gao, J.H., Fung, J.C.H., Wang, S.Y., Li, Y.J., et al., 2020. Source apportionment of secondary organic aerosols in the Pearl River Delta region: Contribution from the oxidation of semi-volatile and intermediate volatility primary organic aerosols. Atmos. Environ. 222, 10.
Yee, L.D., Craven, J.S., Loza, C.L., Schilling, K.A., Ng, N.L., Canagaratna, M.R., et al., 2012. Secondary organic aerosol formation from low-NO(x) photooxidation of dodecane: evolution of multigeneration gas-phase chemistry and aerosol composition. J. Phys. Chem. A 116, 6211–6230.
Yee, L.D., Craven, J.S., Loza, C.L., Schilling, K.A., Ng, N.L., Canagaratna, M.R., et al., 2013. Effect of chemical structure on secondary organic aerosol formation from C_{12} alkanes. Atmos. Chem. Phys. 13, 11121–11140.
Young, C.J., Washenfelder, R.A., Edwards, P.M., Parrish, D.D., Gilman, J.B., Kuster, W.C., et al., 2014. Chlorine as a primary radical: evaluation of methods to understand its role in initiation of oxidative cycles. Atmos. Chem. Phys. 14, 3427–3440.
Yuan, B., Hu, W.W., Shao, M., Wang, M., Chen, W.T., Lu, S.H., et al., 2013. VOC emissions, evolutions and contributions to SOA formation at a receptor site in eastern China. Atmos. Chem. Phys. 13, 8815–8832.
Yuan, B., Koss, A., Warneke, C., Gilman, J.B., Lerner, B.M., Stark, H., et al., 2016. A high-resolution time-of-flight chemical ionization mass spectrometer utilizing hydronium ions (H_3O^+ ToF-CIMS) for measurements of volatile organic compounds in the atmosphere. Atmos. Meas. Tech. 9, 2735–2752.
Zhao, B., Wang, S., Donahue, N.M., Jathar, S.H., Huang, X., Wu, W., et al., 2016. Quantifying the effect of organic aerosol aging and intermediate-volatility emissions on regional-scale aerosol pollution in China. Sci. Rep. 6, 28815.
Zhao, Y., Hennigan, C.J., May, A.A., Tkacik, D.S., de Gouw, J.A., Gilman, J.B., et al., 2014. Intermediate-volatility organic compounds: a large source of secondary organic aerosol. Environ. Sci. Technol. 48, 13743–13750.
Zhao, Y., Kreisberg, N.M., Worton, D.R., Teng, A.P., Hering, S.V., Goldstein, A.H., 2013. Development of an in situ thermal desorption gas chromatography instrument for quantifying atmospheric semi-volatile organic compounds. Aerosol Sci. Technol. 47, 258–266.
Zhao, Y., Nguyen, N.T., Presto, A.A., Hennigan, C.J., May, A.A., Robinson, A.L., 2015. Intermediate volatility organic compound emissions from on-road diesel vehicles: Chemical composition, emission factors, and estimated secondary organic aerosol production. Environ. Sci. Technol. 49, 11516–11526.
Zhou, J., Wang, T., Huang, Y., Mao, T., Zhong, N., Zhang, Y., et al., 2004. Tracing study on pollutants and size distribution of n-alkanes in airborne particles in Beijing area. J. Univ. Pet. China 28 (130), 121–125.